IJMMM International Journal of Minerals, Metallurgy and Materials 矿物冶金与材料学报（英文版）

Effect of Ca/Mg molar ratio on the calcium-based sorbents

Yumeng Li, Qing Zhao, Xiaohui Mei, Chengjun Liu, Henrik Saxén, and Ron Zevenhoven

Cite this article as:
Yumeng Li, Qing Zhao, Xiaohui Mei, Chengjun Liu, Henrik Saxén, and Ron Zevenhoven, Effect of Ca/Mg molar ratio on the calcium-based sorbents, *Int. J. Miner. Metall. Mater.*, 30(2023), No. 11, pp. 2182-2190. https://doi.org/10.1007/s12613-023-2657-y

---

Articles you may be interested in

Xiao-hui Ning, Chen-zheng Liao, and Guo-qing Li, Electrochemical properties of Ca–Pb electrode for calcium-based liquid metal batteries, *Int. J. Miner. Metall. Mater.*, 27(2020), No. 12, pp. 1723-1729. https://doi.org/10.1007/s12613-020-2150-9

Yuan Li, Li-na Cheng, Wen-kang Miao, Chun-xiao Wang, De-zhi Kuang, and Shu-min Han, Nd–Mg–Ni alloy electrodes modified by reduced graphene oxide with improved electrochemical kinetics, *Int. J. Miner. Metall. Mater.*, 27(2020), No. 3, pp. 391-400. https://doi.org/10.1007/s12613-019-1880-z

Yan-bing Zong, Wen-hui Chen, Yong Fan, Tai-lin Yang, Zhao-bo Liu, and Da-qiang Cang, Complementation in the composition of steel slag and red mud for preparation of novel ceramics, *Int. J. Miner. Metall. Mater.*, 25(2018), No. 9, pp. 1010-1017. https://doi.org/10.1007/s12613-018-1651-2

Xiao-yi Shen, Yuan-yong Liang, Hong-mei Shao, Yi Sun, Yan Liu, and Yu-chun Zhai, Extraction and kinetic analysis of Pb and Sr from the leaching residue of zinc oxide ore, *Int. J. Miner. Metall. Mater.*, 28(2021), No. 2, pp. 201-209. https://doi.org/10.1007/s12613-020-1972-9

Sajjad Ali, Yaseen Iqbal, Inamullah Khan, Ansar Ullah, Muhammad Sadiq, Muhammad Fahad, and Khizar Hussain Shah, Hydrometallurgical leaching and kinetic modeling of low-grade manganese ore with banana peel in sulfuric acid, *Int. J. Miner. Metall. Mater.*, 28(2021), No. 2, pp. 193-200. https://doi.org/10.1007/s12613-020-2069-1

Xiao-man Tian, Shen-xu Bao, and Yi-min Zhang, Adsorption properties of V(IV) on resin-activated carbon composite electrodes in capacitive deionization, *Int. J. Miner. Metall. Mater.*, 28(2021), No. 11, pp. 1777-1787. https://doi.org/10.1007/s12613-020-2100-6

IJMMM WeChat

QQ author group

International Journal of Minerals, Metallurgy and Materials
Volume 30, Number 11, November 2023, Page 2182
https://doi.org/10.1007/s12613-023-2657-y

Effect of Ca/Mg molar ratio on the calcium-based sorbents

Yumeng Li[1,2], *Qing Zhao*[1,2,3)✉], *Xiaohui Mei*[1,2], *Chengjun Liu*[1,2], *Henrik Saxén*[4], *and Ron Zevenhoven*[4]

1) Key Laboratory for Ecological Metallurgy of Multimetallic Mineral (Ministry of Education), Northeastern University, Shenyang 110819, China
2) School of Metallurgy, Northeastern University, Shenyang 110819, China
3) Institute for Frontier Technologies of Low-Carbon Steelmaking, Northeastern University, Shenyang 110819, China
4) Process and Systems Engineering Laboratory, Åbo Akademi University, Åbo/Turku 20500, Finland
(Received: 15 February 2023; revised: 7 April 2023; accepted: 18 April 2023)

Abstract: Steelmaking industry faces urgent demands for both steel slag utilization and CO_2 abatement. Ca and Mg of steel slag can be extracted by acid solution and used to prepare sorbents for CO_2 capture. In this work, the calcium-based sorbents were prepared from stainless steel slag leachate by co-precipitation, and the initial CO_2 chemisorption capacity of the calcium-based sorbent prepared from steel slag with the Ca and Mg molar ratio of 3.64:1 was 0.40 g/g. Moreover, the effect of Ca/Mg molar ratio on the morphology, structure, and CO_2 chemisorption capacity of the calcium-based sorbents were investigated. The results show that the optimal Ca/Mg molar ratio of sorbent for CO_2 capture was 4.2:1, and the skeleton support effect of MgO in calcium-based sorbents was determined. Meanwhile, the chemisorption kinetics of the sorbents was studied using the Avrami-Erofeev model. There were two processes of CO_2 chemisorption, and the activation energy of the first stage (reaction control) was found to be lower than that of the second stage (diffusion control).

Keywords: steel slag; carbon dioxide capture; sorbent; chemisorption; kinetics

1. Introduction

In 2021, the crude steel output of China was 1.035 billion tons, ranking first in the world [1]. The production of one ton of crude steel yields about 1.9 t of CO_2 emissions. Carbon emissions in the steel industry accounted for 15% of the total carbon emissions in various industries [2], the steel industry is thus a significant source of carbon dioxide emissions [3–4]. The utilization yield of steel slag in China is only 30% [5–6]. Therefore, to achieve the goal of "carbon peak, carbon neutrality", the implementation of green low-carbon production in the steel industry is imminent [7].

In the long term, CO_2 capture, utilization, and storage (CCUS) technologies are considered to be of great strategic importance for achieving large-scale CO_2 emission reductions [8]. Researchers have carried out systematic research on CO_2 capture and separation based on the calcium cycle (CaL) technology. The use of calcium-based sorbents for CO_2 chemisorption has great potential due to the low cost, availability of CaO, and high capacity for CO_2 chemisorption. The common calcium sources of sorbents include calcium oxide, calcium carbonate, calcium gluconate, and calcium lactate [9]. In recent years, many researchers have used waste materials as calcium sources such as egg shells [9–10], calcium carbide slag [11–12], and steel slag [13–14] to prepare calcium-based sorbent materials by physical mixing methods, sol–gel methods [15], and co-precipitation methods [16]. Compared to most other calcium sources, steel slag holds a distinct advantage since the high Ca content and the low treatment costs. However, the calcium-based sorbents prepared from steel slag still face the problems of poor cyclic adsorption stability [17–20]. Li *et al*. [21] has reported that Mg can act as a structural support in calcium-based sorbents, avoiding pore blockage and improving the stability of the sorbents for CO_2 chemisorption. Therefore, extracting Ca and Mg from steel slag by acid leaching and preparing a MgO doping calcium-based sorbents is a promising method.

Stainless steel slag contains some chromium, which could release along with the Ca and Mg during leaching process causing troublesome pollution issues [22]. To limit the leaching of chromium, stabilization treatment of chromium in stainless steel slag is extremely necessary. A large number of experimental results [23–28] have proved that the molten stainless steel slag can be modified by enriching the toxic Cr elements in stainless steel slag in a stable spinel phase, while the Ca- and Mg-containing elements can be enriched in the easily leached silicate phase for subsequent leaching to recover Ca and Mg. On the basis of these findings, stainless steel slag could also be treated as ordinary steel slag after modification, such as to prepare calcium-based sorbents. However, the compositions of various slags are different resulting the vary contents of Ca, Mg, Si, and Al in slag leachate. Many experiments have shown that Si and Al in sorbents were not harmful components, and hardly affect the

✉ Corresponding author: Qing Zhao E-mail: zhaoq@smm.neu.edu.cn

cyclic chemisorption behavior of Ca [29–31]. researchers [32–35] have found that the CO_2 chemisorption capacity of the sorbent was closely related to the doping content of magnesium in sorbent. Therefore, researches are necessary to investigate the effect of Mg content on the CO_2 chemisorption behavior of calcium-based sorbents, providing a guidance for further effective treatment of steel slag.

In this work, the calcium-based sorbents were prepared from solutions with different Ca/Mg molar ratios to investigate the effects of MgO doping on the sorbent morphology, structure, and CO_2 chemisorption capacity. Moreover, the chemisorption kinetics of the sorbents were studied using the Avrami-Erofeevf model. Meanwhile, the CO_2 chemisorption capacity of the sorbent prepared from stainless steel slag leachate was studied.

2. Experimental

2.1. Preparation of calcium-based sorbents

Calcium-based sorbents were prepared using a co-precipitation method, as shown in Fig. 1. Ca and Mg mixtures with molar ratios of 2, 4, 6, and 8 were prepared using the pure (> 99.9%) $CaCl_2$ (0.5 mol/L) and $MgCl_2$ (0.25–0.625 mol/L). The choice of molar ratio of Ca and Mg mixtures was based on the leaching results of steel slags, including the stainless steel slag [36–37]. An excess of 2 mol/L ammonium carbonate ($(NH_4)_2CO_3$) solution (156 mL) was added to the mixed solution (250 mL), and ammonia (NH_4OH) was added to adjust the pH value of the solution to about 9.8 [38], which is favorable for the production of $CaCO_3$ and $MgCO_3$. Room temperature was performed throughout the process. The mixed solution was filtered after solid–liquid partitioning. The sorbent precursors were obtained by drying the precipitated product in an oven at 120°C for 4 h. The sorbents (xCaO·MgO, x = 2, 4, 6, 8) were obtained by calcining in a muffle furnace at 850°C for 2 h.

2.2. Characterization

Analysis of the thermal weight loss of the sorbent precursors at different temperatures was carried out by heating the samples from room temperature to 1000°C at a rate of 10°C/min in Ar atmosphere using a thermogravimetric analyzer (TG-DSC, SDTQ600). The appearance and chemical composition of the samples were observed by scanning electron microscope and energy dispersive spectrometer (SEM–EDS, ZEISS EVO18). The phase composition of the sorbent was examined by using an X-ray diffractometer (XRD, Bruker D8 Advance) with a sweeping range of 2θ = 10°–90° and a tracing speed of 8°/min. N_2 adsorption–desorption isotherms of the samples were measured at liquid nitrogen temperature using a physical adsorption analyzer (Micromeritics Tristar Ⅱ 3020) with the samples degassed at 200°C for 6 h to remove the impurities from the pores. The specific surface area, pore volume, and average pore size of the samples were calculated by Brunner–Emmet–Teller and Barret–Joyner–Halenda (BJH).

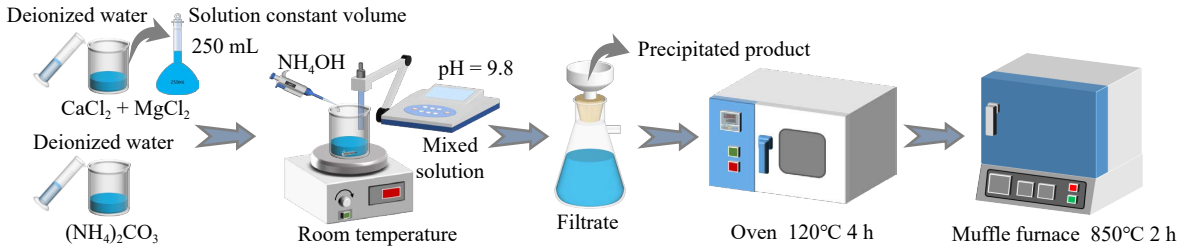

Fig. 1. Diagram of the preparation process for calcium-based sorbents by co-precipitation.

2.3. CO_2 chemisorption test

The CO_2 chemisorption experiment was tested by Mettler-Toledo TGA/DSC3+ at ambient pressure (1.0 atm) under the conditions shown in Fig. 2.

The carbonation conversion yield and CO_2 chemisorption capacity per unit mass of sorbent were calculated from the experimentally obtained data by Eqs. (1) and (2).

$$X_N = \frac{m_N - m_0}{m_0 \cdot a} \times \frac{M_{CaO}}{M_{CO_2}} \times 100\% \quad (1)$$

$$Y_N = \frac{m_N - m_0}{m_0} \quad (2)$$

where X_N is the carbonation conversion yield of the sorbent (%), Y_N is the CO_2 chemisorption capacity per unit mass of the sorbent (g/g), N is the number of cycles, m_0 is the initial mass of the sorbent (g), a is the mass fraction of the active CaO in the sorbent (%), m_N is the mass of the sorbent after the Nth cycle (g), M_{CaO} is the molar mass of CaO (g/mol), and M_{CO_2} is the molar mass of CO_2 (g/mol).

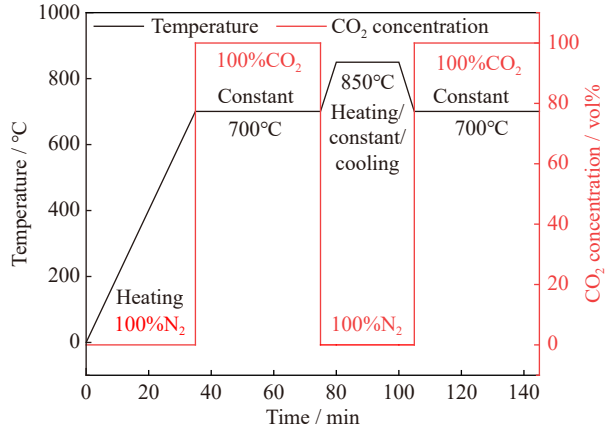

Fig. 2. CO_2 single/cyclic chemisorption experimental operation of the sorbent.

3. Results and discussion

3.1. Structural characteristics of the sorbents

The contents of Ca^{2+} and Mg^{2+} in the filtrate of the sorbents, named 2CaO·MgO, 4CaO·MgO, 6CaO·MgO, and 8CaO·MgO, were determined by titrating by ethylene diamine tetraacetie acid standard solution [39], with results shown in Table 1.

Fig. 3(a) shows the TG-DSC test results of the sorbent precursor. The sample experienced three weight loss periods during the heating process, corresponding to three peaks in the heat flow curve. The weight loss below 300°C is due to the removal of crystal water, the weight loss between 300 and 500°C is caused by the decomposition of $MgCO_3$, and the weight loss at about 700°C is the decomposition of $CaCO_3$. Based on this, to ensure that the samples are completely calcined from $CaCO_3$ to CaO, 850°C was selected as the calcination temperature.

Table 1. Theoretical and actual Ca/Mg molar ratio of the sorbents

Theoretical Ca/Mg molar ratio	Ca^{2+} transformation yield / %	Mg^{2+} transformation yield / %	Actual Ca/Mg molar ratio
2:1	99.84	96.40	2.1:1
4:1	99.84	95.52	4.2:1
6:1	99.68	94.24	6.3:1
8:1	99.68	93.60	8.5:1

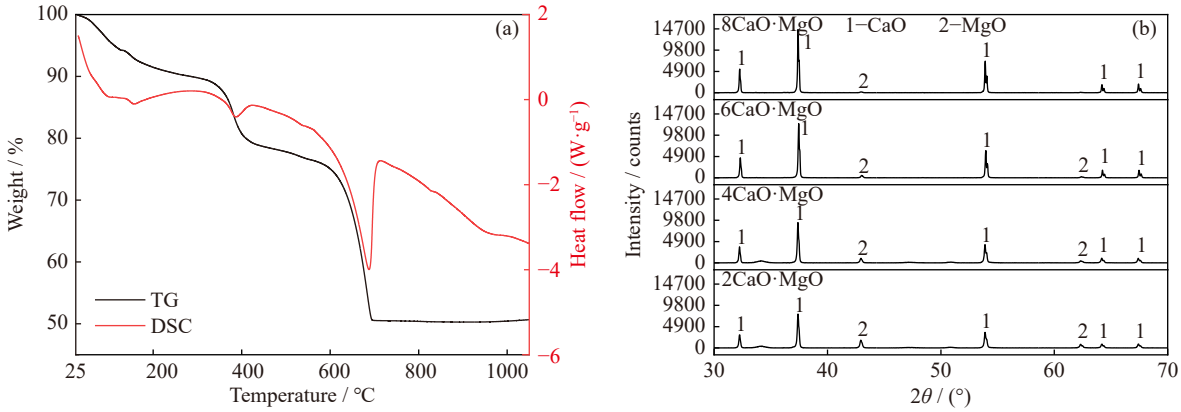

Fig. 3. (a) Thermal weight loss curve and heat flow curve of the sorbent precursor and (b) XRD patterns of the sorbents with different Ca/Mg molar ratios.

Fig. 3(b) shows the XRD pattern of the sorbents. The main phases in the sorbent are CaO and MgO. With the increase of MgO doping content, the intensity of CaO diffraction peak gradually decreases, resulting in poor crystallization and small grain size of CaO. There is no obvious shift in the peak position of CaO, which indicates that the doped MgO does not enter the interior of the CaO lattice, but instead that a simple physical mixture of the two component arises during the preparation of the sorbent [34,40].

The average grain sizes of CaO in the sorbent were calculated by the Scherrer equation:

$$\beta = \frac{k \cdot \lambda}{D_{hkl} \cdot \cos\theta} \tag{3}$$

where D_{hkl} is the grain size perpendicular to the crystal plane (hkl), k is a constant, taken as 0.89 when applying half-height peak width and 0.94 when applying integral peak width. Using Cu K_α radiation, λ equal to 0.15406 nm, β is the radian value corresponding to the half-peak width, and θ is the diffraction angle.

Table 2 shows that the average grain sizes of CaO in 8CaO·MgO, 6CaO·MgO, 4CaO·MgO, and 2CaO·MgO sorbents perpendicular to the (111), (200), and (220) crystal planes are 49.4, 47.7, 44.0, and 42.2 nm, respectively. The average grain size of CaO gradually decreases with the increase of MgO doping, indicating that doping effectively prevents the agglomeration and growth of CaO crystallites.

Table 2. CaO average grain size of the sorbents

Sorbent	D_{hkl} / nm			$\bar{D}$/nm
	(111)	(200)	(220)	
CaO	53.0	49.0	39.6	47.2
8CaO·MgO	55.9	51.2	40.3	49.4
6CaO·MgO	55.9	50.7	40.0	47.7
4CaO·MgO	50.5	45.9	35.6	44.0
2CaO·MgO	48.5	43.8	34.3	42.2

Note: $\bar{D}$ represents the average grain sizes of CaO in sorbents.

As shown in Fig. 4, the isothermal N_2 chemisorption and desorption curves of the sorbents are all of type IV, with the pore size primarily around 8 nm, which represents mesoporous materials. The pore characteristics parameters in Table 3 indicate that compared to other calcium-based sorbents, the 4CaO·MgO and 6CaO·MgO sorbents have a larger specific surface area and pore volume: the larger the specific surface area, the more adsorption sites are provided by the sorbent surface, and the stronger is the chemisorption capacity.

The SEM image and EDS element mapping results in Fig. 5 show that the MgO doping has an effect on the surface morphology and the three elements Ca, Mg, and O are uniformly distributed in the sorbent. Combined with the findings of Table 3, it can be concluded that the sorbents with relatively larger specific surface area and pore volume have a loose and porous surface morphology, while the sorbents

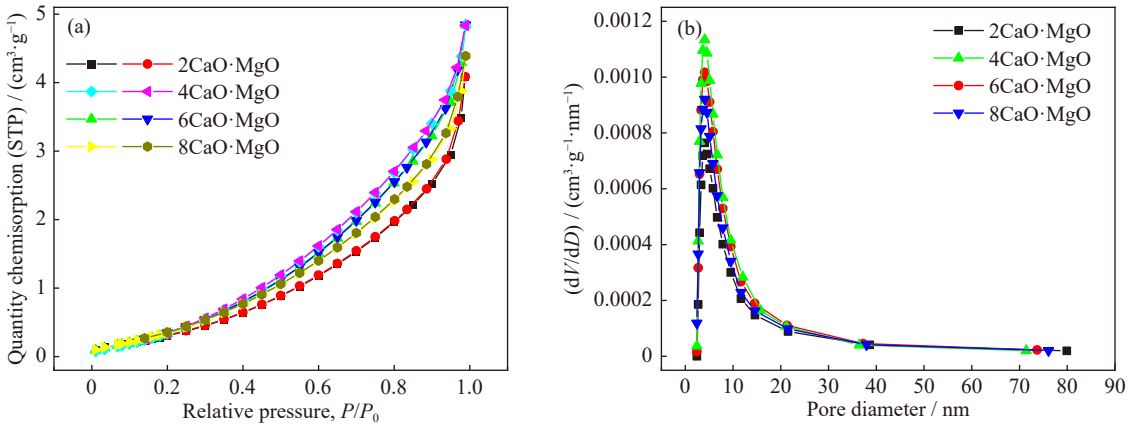

Fig. 4. Isothermal chemisorption–desorption curve (a) and pore size distribution (b) for the sorbents. STP means standard temperature and pressure; d*V*/d*D* represents pore volume per unit pore size.

Table 3. Pore characteristic parameters of the sorbents

Sorbent	Specific surface area / ($m^2 \cdot g^{-1}$)	BJH pore size / nm	BJH pore volume / ($cm^3 \cdot g^{-1}$)
2CaO·MgO	1.4782	8.6565	0.006752
4CaO·MgO	2.3243	7.4672	0.008737
6CaO·MgO	1.9614	7.9290	0.008246
8CaO·MgO	1.9339	7.8946	0.007263

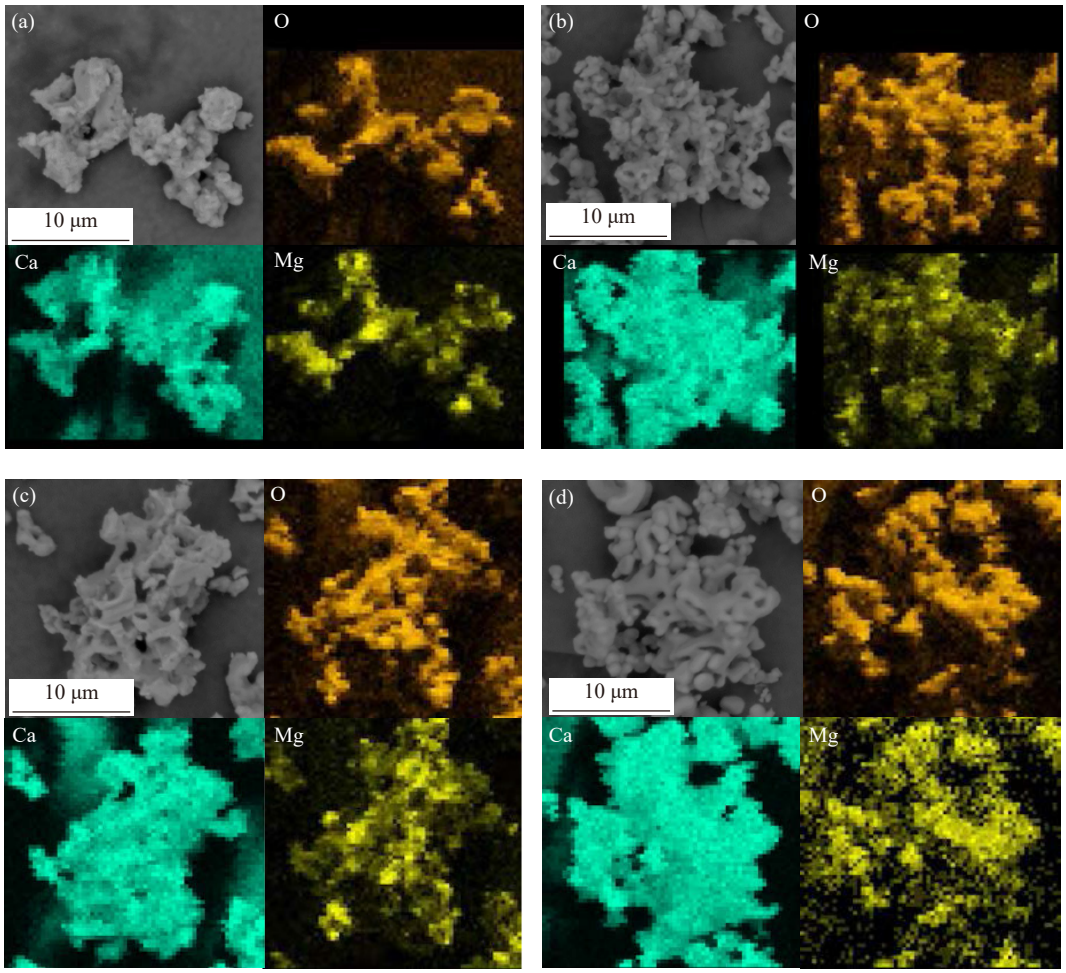

Fig. 5. SEM images and EDS element mapping results of the sorbents (a) 2CaO·MgO, (b) 4CaO·MgO, (c) 6CaO·MgO, and (d) 8CaO·MgO.

with smaller specific surface area and pore volume have a dense and smooth surface morphology. During the CO_2 chemisorption reaction, the loose and porous surface structure facilitates the diffusion of CO_2 into the interior of the sorbent and the subsequent chemisorption reaction.

3.2. CO_2 single chemisorption of the sorbents

3.2.1. Effect of MgO doping content

$MgCO_3$ is decomposed into MgO and CO_2 at above around 410°C at atmospheric pressure in Fig. 3(a). Under the experimental conditions set here, the chemisorption temperature is 700°C and the desorption temperature is 850°C, both much higher than the decomposition temperature of $MgCO_3$. Fig. 6 clearly shows that MgO cannot react with CO_2, so it is considered to be an inert component [31].

Fig. 7 shows the chemisorption capacity of the sorbents for a long CO_2 chemisorption period. The CO_2 chemisorption capacity of the sorbents increased with the increase of MgO doping content in the first 20 min. At 20 min, the 2CaO·MgO sorbent had the highest CO_2 chemisorption capacity of 0.3 g/g, indicating that the increase of MgO doping content is beneficial to increase the initial CO_2 chemisorption capacity. However, as the chemisorption time increases, the 4CaO·MgO sorbent shows better chemisorption performance, which may be related to its large specific surface area and the number of chemisorption sites provided [41–42]. The 8CaO·MgO sorbent consistently shows the lowest CO_2 chemisorption capacity. Thus, a very high or very low MgO doping content is not beneficial for the CO_2 chemisorption by the sorbents.

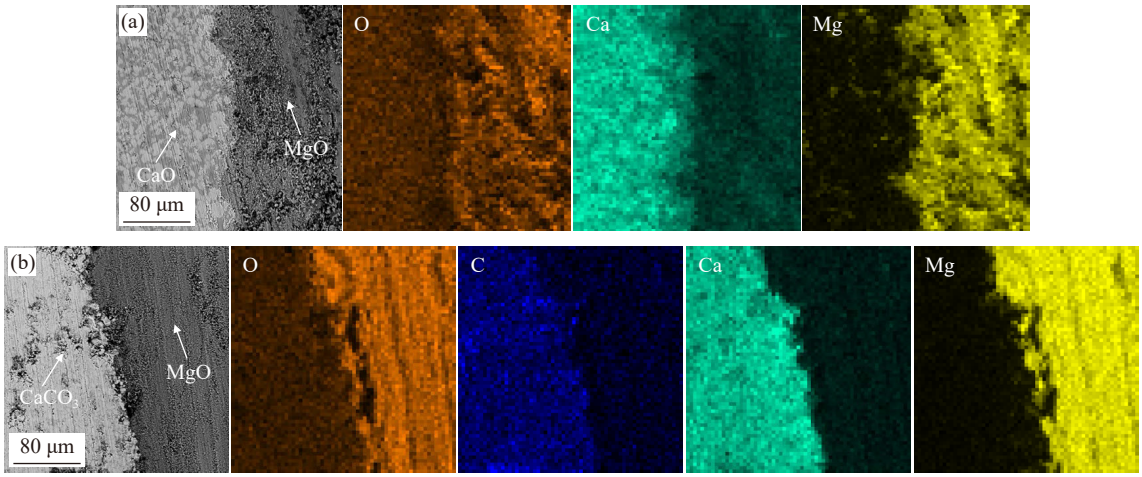

Fig. 6. SEM images and EDS element mapping results of the blocky CaO·MgO sorbent before (a) and after (b) CO_2 chemisorption.

3.2.2. Kinetic chemisorption of the sorbent

Based on the results presented in Fig. 7, the kinetics of the chemisorption capacity of the 4CaO·MgO sorbent for a long CO_2 chemisorption can be further analyzed. The adsorption is a gas–solid two-phase reaction, and the kinetic process was analyzed by the constant temperature adsorption method. Khoshandam *et al.* [43] divided the process of CaO chemisorption of CO_2 into two stages, the first controlled by chemical reactions and the second controlled by diffusion

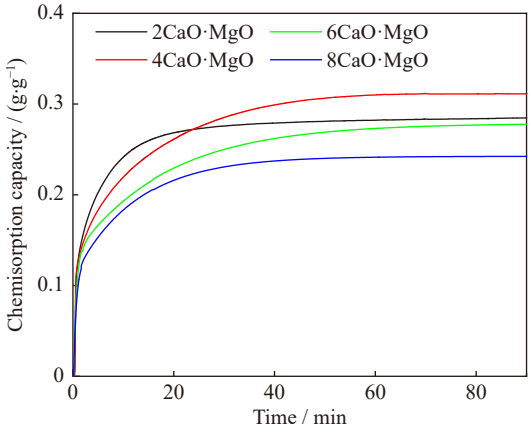

Fig. 7. Chemisorption capacity of the sorbents.

[44]. Fig. 8(a)–(c) presents the chemisorption capacity, the carbonation conversion X, and its time derivative dX/dt for sorbents, respectively. Fig. 8(c) clearly shows that the reaction is very fast at the beginning of the carbonation due to the reaction between CO_2 and the directly exposed surface of the sorbent, and the reaction rate reaches its highest value point P_1. As the reaction continues, the $CaCO_3$ product layer starts forming and gradually thickens. The appearance of this product layer hinders the reaction between CO_2 and the unreacted CaO inside the sorbent, increasing the diffusion resistance and slowing down the reaction. The reaction rate is already low when the reaction has proceeded to P_2 (about 8%/min), after which the reaction enters a slower stage.

The kinetic simulation of the CO_2 chemisorption process of sorbent was carried out by using the kinetic model equation (Eq. (4)) for a constant temperature, the Arrhenius equation (Eq. (5)), and the Avrami-Erofeev model (Eq. (6)) [42].

$$\frac{dX}{dt} = K \cdot F(X) \tag{4}$$

$$K = K_0 \cdot \exp[-E/(RT)] \tag{5}$$

$$F(X) = (1/n)(1-X)[-\ln(1-X)]^{-(n-1)} \tag{6}$$

where X is the carbonation conversion yield of the sorbent, K is the reaction rate constant, T is the chemisorption temperat-

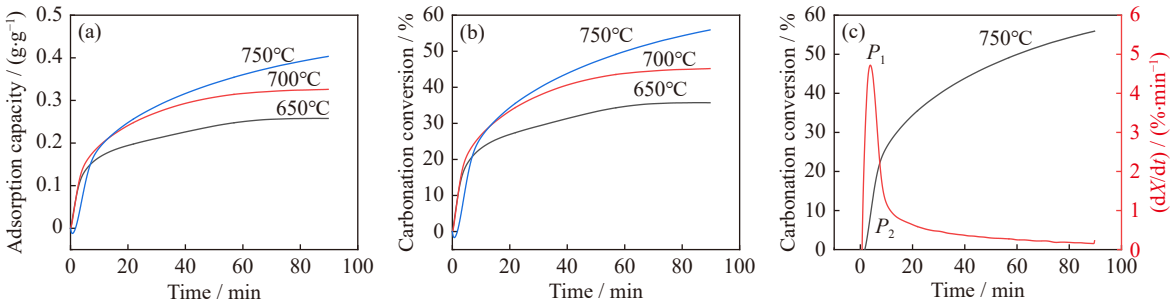

Fig. 8. Chemisorption capacity (a), carbonation conversion *X* (b), and conversion gradient (d*X*/d*t*) (c) for sorbents at different chemisorption temperatures.

ure, K_0 is the pre-exponential factor, E is the activation energy, R is the gas constant and equal to 8.314 J/(mol·K), and reaction order n equal to 1/4–4.

The Eq. (6) was fitted to the experimental results by the methods of least squares. Tables S1 and S2 giving the r^2 values for different reaction orders n of the first and second stages. Table S3 presents the values of K and $-\ln K$ at different temperatures, while Fig. 9 plots $-\ln K$ against $1/(T\times 10^{-3})$ for the different stages and a linear fit. The slope of this curve is $-E/R$ and the intercept is $-\ln K_0$. From these, the activation energy E and the pre-exponential factor K_0 are obtained.

The results in Table 4 show that the activation energy of the first stage is less than that of the second stage. In fact, the lower the activation energy, the faster the reaction rate. Therefore, the reaction rate of second stage is lower than that of first stage. The activation energy tells the temperature dependence. As is seen, the value of E increases with an increase T. There is a relationship of mutual compensation between the activation energy and the pre-exponential factor, called the "compensation effect", which is caused by the fact that the problem is somewhat ill-conditioned [45–46]: According to Arrhenius model Eq. (5) there is a linear relationship between the activation energy E and the logarithm of pre-exponential factor K_0, as shown in Eq. (7), the higher the value of the activation energy E, the higher the value of the pre-exponential factor K_0.

$$\ln K_0 = aE + b \tag{7}$$

where a and b are slope and intercept, and a > 0.

The carbonation reaction of the sorbent conforms to the nucleation and growth mechanism of the Aveami-Erofeev model. The linear relationship of the fitted curve is determined by the r^2 values for different reaction orders n of the first and second stages (Tables S1 and S2). Therefore, the model of n = 2/3 is determined by fitting in the first stage (reaction control), and the model of n = 1/2 is determined by fitting in the second stage (diffusion control).

3.3. CO_2 regeneration chemisorption of the sorbents

Fig. 10(a) shows the CO_2 chemisorption capacity of the first chemisorption and the second chemisorption of the different Ca/Mg molar ratio sorbents. After the second chemisorption of CO_2, the chemisorption capacity of the sorbents increased substantially compared to the first chemisorption, and 4CaO·MgO shows a maximum CO_2 chemisorption capacity of 0.60 g/g. This phenomenon is known as the "self-reactivation" phenomenon of the sorbents [47]. The occurrence of self-activation is mainly related to the structural changes of the sorbents, and Manovic and An-

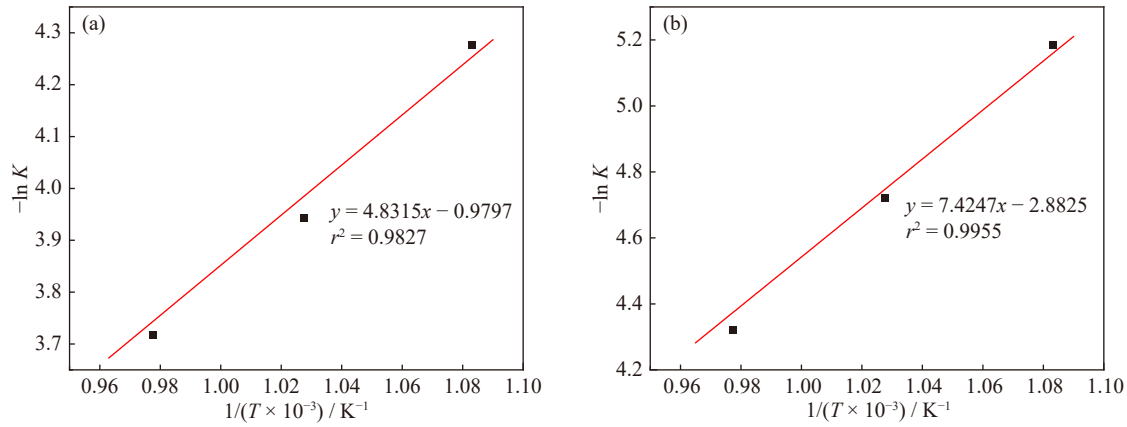

Fig. 9. Relationship between ln *K* and 1/(*T* × 10^{-3}) of (a) the first stage and (b) the second stage of the chemisorption process. r^2 means the degree of fit.

Table 4. Activation energy *E* and pre-exponential factor K_0 of the different stages of the chemisorption

First stage		Second stage	
Activation energy *E* / (kJ·mol^{-1})	Pre-exponential factor K_0	Activation energy *E* / (kJ·mol^{-1})	Pre-exponential factor K_0
40.17	2.66	61.73	17.86

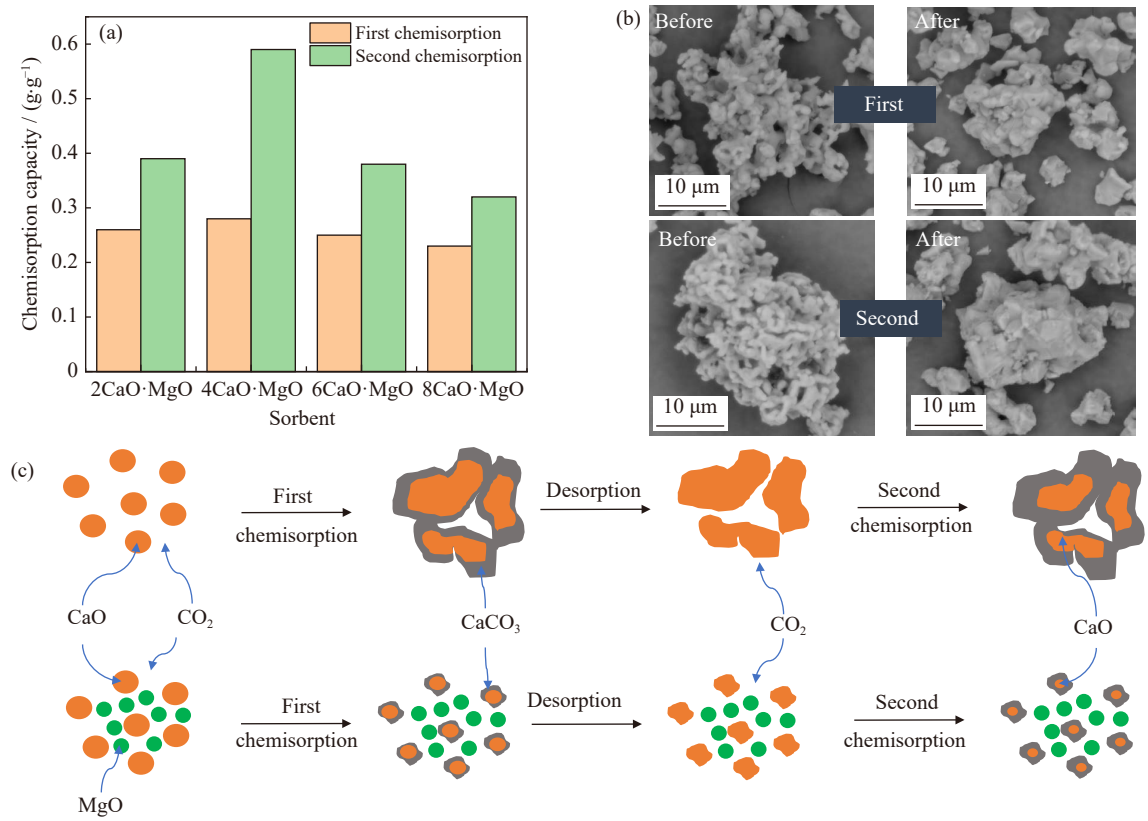

Fig. 10. CO_2 chemisorption capacity at 700°C (a), SEM images (b), and schematic of the process (c) of the first and second chemisorption of the sorbents.

thony [47] explained this phenomenon: In the preparation of the sorbents, the sorbent precursor is calcined at high temperatures to form a sorbent containing the inert component MgO. The sorbent forms a hard skeleton on the inside and a soft skeleton on the outside. The soft skeleton shows CO_2 chemisorption performance, but the hard skeleton does not. However, the hard skeleton can play a skeleton support role inside the sorbent, which helps to maintain the stability of the pore structure of the sorbent. After CO_2 chemisorption–desorption using the sorbent, the hard skeleton gradually transforms into a soft skeleton with CO_2 chemisorption activity, and the doping of the inert component MgO also helps to prolong the self-reactivation cycle of the sorbents, as shown by a gradual increase in CO_2 chemisorption capacity during the first few cycles.

With reference to Fig. 10(b) and (c), it may be concluded that before the chemisorption of CO_2, the small particles of sorbent gathered with each other and formed irregular deposits with obvious holes. After the chemisorption of CO_2, the sorbent generated carbonate products from the outside to the inside, and the outer surface is covered by carbonate product layers, which is a dense block structure. After the desorption of CO_2, the morphology of the regenerated sorbent is fluffier showing more developed pores than the initial sorbent. As an inert component, MgO plays a supporting role in the sorbent, which is also one of the reasons for the higher CO_2 chemisorption capacity of the sorbent during the second chemisorption. Therefore, to increase the CO_2 chemisorption capacity of the sorbent, the first chemisorption process step is used as a pretreatment stage.

3.4. Calcium-based sorbent prepared from steel slag

According to the process in Fig. 1, mixed solution was replaced by the stainless steel slag leachate and the calcium-based sorbent was prepared directly. Fig. S1 shows the SEM image and EDS element mapping result of the calcium-based sorbent form stainless steel slag, the main elements in the sorbent are Ca and Mg, and Si and Al are relatively less. The initial CO_2 chemisorption capacity of the calcium-based sorbent after pretreatment is calculated by Eq. (2) to be 0.40 g/g and is a very promising raw material for the CCUS.

Table 5 shows the CO_2 chemisorption capacity of the sorbents prepared by different Ca/Mg molar ratio mixture

Table 5. Comparison of CO_2 chemisorption capacity of calcium-based sorbents

Raw material	Preparation method	Temperature / (°C)	Ca/Mg molar ratio	CO_2 chemisorption capacity / ($g \cdot g^{-1}$)
Stainless steel slag	Co-precipitation	700	3.64:1	0.40
$CaCl_2$+$MgCl_2$	Co-precipitation	700	2.1:1	0.39
			4.2:1	0.60
			6.3:1	0.38
			8.5:1	0.32

solutions and stainless steel leachate. The CO_2 chemisorption capacity of calcium-based sorbent prepared from the stainless steel slag leachate is lower than that prepared from mixture solution with Ca/Mg molar ratio of 4.2:1, which may be related to the presence of impurity elements in the adsorbent. At present, the mechanisms of action of Si and Al on CO_2 chemisorption capacity in sorbents is still in the research stage and will be reported accordingly in the future.

4. Conclusions

In this study, the calcium-based sorbents were prepared, and the effect of Ca/Mg molar ratios was investigated. The following main conclusions are drawn as follow.

(1) The doping of MgO can reduce the size of CaO grains found by calculating and comparing the microcrystalline parameters of CaO in different sorbents. However, doping with small or large amounts of MgO is not beneficial for the CO_2 chemisorption capacity. Thus, the MgO doping should be carefully designed to achieve maximum benefits and avoid possible drawbacks.

(2) The chemisorption kinetics of the sorbent was studied by the Avrami-Erofeev model. It is demonstrated that the activation energy of the first stage is lower than in the second stage.After regeneration of the sorbent, the CO_2 chemisorption capacity was increased due to the "self-reactivation" phenomenon of the sorbent, and thus the skeleton support effect of MgO in the sorbent could be verified.

(3) The maximum initial CO_2 chemisorption capacity of the sorbent prepared from the mixed solutions with different Ca/Mg molar ratios was 0.60 g/g after pretreatment, and the initial CO_2 chemisorption capacity of the sorbent prepared from the stainless steel slag acid leach solution with the Ca/Mg molar ratio of 3.64:1 was to be 0.40 g/g.

Acknowledgements

This work was financially supported by the National Natural Science Foundation of China (No. 52074078), the National Key R&D Program of China (No. 2021YFC2901200), the Applied Fundamental Research Program of Liaoning Province (No. 2023JH2/101600002), the Liaoning Provincial Natural Science Foundation of China (No. 2022-YQ-09), the Shenyang Young Middle-Aged Scientific and Technological Innovation Talent Support Program, China (No. RC220491), the Liaoning Province Steel Industry-University-Research Innovation Alliance Cooperation Project of Bensteel Group, China (No. KJBLM202202), and the Fundamental Research Funds for the Central Universities, China (Nos. N2201023 and N2325009).

Conflict of Interest

Qing Zhao is a youth editorial board member for IJMMM and is not involved in the editorial review or the decision to publish this article. All authors declare no competing financial interest.

Supplementary Information

The online version contains supplementary material available at https://doi.org/10.1007/s12613-023-2657-y

References

[1] J. Su, Y.B. Liang, L. Ding, G.S. Zhang, and H. Liu, Research on China's energy development strategy under carbon neutrality, *Bull. Chin. Acad. Sci.*, 36(2021), No. 9, p. 1001.

[2] W.L. Dong, G.H. Ding, A.J. Xu, *et al*., Development of CO_2 capture and utilization technology in steelmaking plant, *Iron Steel Res. Int.*, (2023). DOI: 10.1007/s42243-023-00927-3

[3] H.X. Zhang, W.Q. Sun, W.D. Li, and G.Y. Ma, A carbon flow tracing and carbon accounting method for exploring CO_2 emissions of the iron and steel industry: An integrated material–energy–carbon hub, *Appl. Energy*, 309(2022), art. No. 118485.

[4] L.Y. Liu, H.G. Ji, X.F. Lü, *et al*., Mitigation of greenhouse gases released from mining activities: A review, *Int. J. Miner. Metall. Mater.*, 28(2021), No. 4, p. 513.

[5] J.L. Guo, Y.P. Bao, and M. Wang, Steel slag in China: Treatment, recycling, and management, *Waste Manage.*, 78(2018), p. 318.

[6] H. Matsuura, X. Yang, G. Li, Z. Yuan, and F. Tsukihashi, Recycling of ironmaking and steelmaking slags in Japan and China, *Int. J. Miner. Metall. Mater.*, 29(2022), No. 4, p. 739.

[7] Z.F. Cui, A.J. Xu, and F.Q. Shang Guan, Low-carbon development strategy analysis of the domestic and foreign steel industry, *Chin. J. Eng.*, 44(2022), No. 9, p. 1496.

[8] A.J. Nathanael, K. Kannaiyan, A.K. Kunhiraman, S. Ramakrishna, and V. Kumaravel, Global opportunities and challenges on net-zero CO_2 emissions towards a sustainable future, *React. Chem. Eng.*, 6(2021), No. 12, p. 2226.

[9] W.Q. Liu, N.W.L. Low, B. Feng, G. Wang, and J.C. Diniz da Costa, Calcium precursors for the production of CaO sorbents for multicycle CO_2 capture, *Environ. Sci. Technol.*, 44(2010), No. 2, p. 841.

[10] T. Witoon, Characterization of calcium oxide derived from waste eggshell and its application as CO_2 sorbent, *Ceram. Int.*, 37(2011), No. 8, p. 3291.

[11] Y.J. Li, R.Y. Sun, C.T. Liu, H.L. Liu, and C.M. Lu, CO_2 capture by carbide slag from chlor-alkali plant in calcination/carbonation cycles, *Int. J. Greenhouse Gas Control*, 9(2012), p. 117.

[12] Y.J. Li, R.Y. Sun, H.L. Liu, and C.M. Lu, Reactivation properties of carbide slag as a CO_2 sorbent during calcination/carbonation cycles, [in] H.Y. Qi and B. Zhao, eds., *Cleaner Combustion and Sustainable World*, Berlin, 2013, p. 1233.

[13] S.C. Tian, J.G. Jiang, F. Yan, K.M. Li, and X.J. Chen, Synthesis of highly efficient CaO-based, self-stabilizing CO_2 sorbents via structure-reforming of steel slag, *Environ. Sci. Technol.*, 49(2015), No. 12, p. 7464.

[14] S.C. Tian, J.G. Jiang, F. Yan, K.M. Li, X.J. Chen, and V. Manovic, Highly efficient CO_2 capture with simultaneous iron and CaO recycling for the iron and steel industry, *Green Chem.*, 18(2016), No. 14, p. 4022.

[15] M. Broda, A.M. Kierzkowska, and C.R. Müller, Application of the sol–gel technique to develop synthetic calcium-based sorbents with excellent carbon dioxide capture characteristics, *ChemSusChem*, 5(2012), No. 2, p. 411.

[16] D. Karami and N. Mahinpey, Highly active CaO-based sorbents for CO_2 capture using the precipitation method: Preparation and characterization of the sorbent powder, *Ind. Eng. Chem. Res.*, 51(2012), No. 12, p. 4567.

[17] H.C. Chen, C.S. Zhao, Y.J. Li, and X.P. Chen, CO_2 capture per-

formance of calcium-based sorbents in a pressurized carbonation/calcination loop, *Energy Fuels*, 24(2010), No. 10, p. 5751.
[18] M. Erans, V. Manovic, and E.J. Anthony, Calcium looping sorbents for CO_2 capture, *Appl. Energy*, 180(2016), p. 722.
[19] J. Miranda-Pizarro, A. Perejón, J.M. Valverde, P.E. Sánchez-Jiménez, and L.A. Pérez-Maqueda, Use of steel slag for CO_2 capture under realistic calcium-looping conditions, *RSC Adv.*, 6(2016), No. 44, p. 37656.
[20] X.Y. Yan, Y.J. Li, J.L. Zhao, and Z.Y. Wang, Density functional theory study on CO_2 adsorption by Ce-promoted CaO in the presence of steam, *Energy Fuels*, 34(2020), No. 5, p. 6197.
[21] L.Y. Li, D.L. King, Z.M. Nie, and C. Howard, Magnesia-stabilized calcium oxide absorbents with improved durability for high temperature CO_2 capture, *Ind. Eng. Chem. Res.*, 48(2009), No. 23, p. 10604.
[22] S. Rodiah, M. Huljana, J.L. Al Jabbar, C. Ichsan, and H. Marzuki, Silica-rice husk as adsorbent of Cr (VI) ions prepared through sol–gel method, *Walisongo J. Chem.*, 4(2021), No. 1, p. 65.
[23] Q. Zhao, C.J. Liu, L.H. Cao, X. Zheng, and M.F. Jiang, Effect of lime on stability of chromium in stainless steel slag, *Minerals*, 8(2018), No. 10, art. No. 424.
[24] Q. Zhao, C.J. Liu, L.H. Cao, X. Zheng, and M.F. Jiang, Stability of chromium in stainless steel slag during cooling, *Minerals*, 8(2018), No. 10, art. No. 445.
[25] Q. Zhao, C.J. Liu, T.C. Gao, L. Gao, H. Saxén, and R. Zevenhoven, Remediation of stainless steel slag with MnO for CO_2 mineralization, *Process. Saf. Environ. Prot.*, 127(2019), p. 1.
[26] Q. Zhao, J.Y. Li, K.W. You, and C.J. Liu, Recovery of calcium and magnesium bearing phases from iron- and steelmaking slag for CO_2 sequestration, *Process. Saf. Environ. Prot.*, 135(2020), p. 81.
[27] Q. Zhao, K. Liu, L.F. Sun, *et al*., Towards carbon sequestration using stainless steel slag via phase modification and co-extraction of calcium and magnesium, *Process. Saf. Environ. Prot.*, 133(2020), p. 73.
[28] L.H. Cao, C.J. Liu, Q. Zhao, and M.F. Jiang, Effect of Al_2O_3 modification on enrichment and stabilization of chromium in stainless steel slag, *J. Iron Steel Res. Int.*, 24(2017), No. 3, p. 258.
[29] D.D. Fang, L.H. Zhang, L.J. Zou, and F. Duan, Effect of leaching parameters on the composition of adsorbents derived from steel slag and their CO_2 capture characteristics, *Greenhouse Gases: Sci. Technol.*, 11(2021), No. 5, p. 924.
[30] S.F. Wu, Q.H. Li, J.N. Kim, and K. B. Yi, Properties of a nano CaO/Al_2O_3 CO_2 sorbent, *Ind. Eng. Chem. res.*, 47(2008), No. 1, p. 180.
[31] M. Broda, A.M. Kierzkowska, and R.C. Muller. Development of highly effective CaO-based, MgO-stabilized CO_2 sorbents via a scalable "one-pot" recrystallization technique, *Adv. Funct. Mater.*, 24(2014), No. 36, p. 5753.
[32] P.Q. Lan and S.F. Wu, Synthesis of a porous nano-CaO/MgO-based CO_2 adsorbent, *Chem. Eng. Technol.*, 37(2014), No. 4, p. 580.
[33] W.Q. Liu, B. Feng, Y.Q. Wu, G.X. Wang, J. Barry, and J.C. Diniz da Costa, Synthesis of sintering-resistant sorbents for CO_2 capture, *Environ. Sci. Technol.*, 44(2010), No. 8, p. 3093.
[34] C. Luo, Y. Zheng, Q.L. Wu, N. Ding, and C. Zheng, Cyclic reaction characters of novel CaO/MgO high temperature CO_2 sorbents, *J. Eng. Thermophys.*, 32(2011), No. 11, p. 1957.
[35] M.A. Naeem, A. Armutlulu, Q. Imtiaz, *et al*., Optimization of the structural characteristics of CaO and its effective stabilization yield high-capacity CO_2 sorbents, *Nat. Commun.*, 9(2018), art. No. 2408.
[36] X.H. Mei, Q. Zhao, Y. Min, C.J. Liu, H. Saxén, and R. Zevenhoven, Phase transition and dissolution behavior of Ca/Mg-bearing silicates of steel slag in acidic solutions for integration with carbon sequestration, *Process. Saf. Environ. Prot.*, 159(2022), p. 221.
[37] X.H. Mei, Q. Zhao, J.Y. Zhou, *et al*., Phase transition of Ca- and Mg-bearing minerals of steel slag in acidic solution for CO_2 sequestration, *J. Sustain. Metall.*, 7(2021), No. 2, p. 391.
[38] X.H. Mei, Q. Zhao, Y.M. Li, *et al*., Phase transition and morphology evolution of precipitated calcium carbonate (PCC) in the CO_2 mineralization process, *Fuel*, 328(2022), art. No. 125259.
[39] R.J. Ferretti and W.M. Hoffman, Determination of calcium and magnesium in mixed fertilizers by EDTA titration, *J. Assoc. Off. Agric. Chem.*, 45(1962), No. 1, p. 22.
[40] C. Luo, Y. Zheng, N. Ding, Q.L. Wu, and C. Zheng, Synthesis and performance of a nano synthetic Ca-based sorbent for high temperature CO_2 capture, *Proc. CESS*, 31(2011), No. 8, p. 45.
[41] H.T. Jang, Y. Park, Y.S. Ko, J.Y. Lee, and B. Margandan, Highly siliceous MCM-48 from rice husk ash for CO_2 adsorption, *Int. J. Greenhouse Gas Control*, 3(2009), No. 5, p. 545.
[42] W.T. Zeng and H. Bai, Swelling-agent-free synthesis of rice husk derived silica materials with large mesopores for efficient CO_2 capture, *Chem. Eng. J.*, 251(2014), p. 1.
[43] B. Khoshandam, R.V. Kumar, and L. Allahgholi, Mathematical modeling of CO_2 removal using carbonation with CaO: The grain model, *Korean J. Chem. Eng.*, 27(2010), No. 3, p. 766.
[44] C.Q. Hu, T. Han, Y.Z. Zhang, and Z.X. Zhang, Theoretical foundation of carbonation pellet process for ferrous sludge recycling, *J. Iron Steel Res. Int.*, 18(2011), No. 12, p. 27.
[45] P.J. Barrie, The mathematical origins of the kinetic compensation effect: 1. the effect of random experimental errors, *Phys. Chem. Chem. Phys.*, 14(2012), No. 1, p. 318.
[46] P.J. Barrie, The mathematical origins of the kinetic compensation effect: 2. the effect of systematic errors, *Phys. Chem. Chem. Phys.*, 14(2012), No. 1, p. 327.
[47] V. Manovic and E.J. Anthony, Thermal activation of CaO-based sorbent and self-reactivation during CO_2 capture looping cycles, *Environ. Sci. Technol.*, 42(2008), No. 11, p. 4170.